

Low-Power Collision Avoidance Memristive Circuit for Swarms of Miniature Robots

Ioannis K. Chatzipaschalis^{*†}, Theodoros Panagiotis Chatzinikolaou^{*}, Emmanuil Stavroulakis^{*}, Evangelos Tsipas^{*}, Iosif-Angelos Fyrigos^{*}, Antonio Rubio[†], and Georgios Ch. Sirakoulis^{*}

^{*} Department of Electrical and Computer Engineering, Democritus University of Thrace, Xanthi, Greece

[†] Department of Electronic Engineering, Universitat Politècnica de Catalunya, Barcelona, Spain

Abstract—A swarm of miniature robots comprises mini-robots collaborating to achieve common goals, inspired by the collective behavior of insects. This concept mimics decentralized cooperation, enabling complex task accomplishment across various fields such as healthcare, exploration, and rescue missions. Mini-robots operate in confined spaces and time frames with minimal energy, requiring efficient path planning to prevent collisions within their group and surroundings. Integrating ultra-low-power electronics in these robots is essential. Memristors, renowned for their low power consumption, simplicity, and high integration density, hold significant promise. This paper proposes an integrated collision avoidance memristive circuit with neuromorphic behavior for miniature robots. This circuit not only enhances swarm efficiency but also lays the groundwork for fully analog mini-robots.

Index Terms—Collision Avoidance, Memristor, Miniature Robots, Memristive Neuromorphic Voltage-Controlled Oscillator (MNVCO), Passive Memristive Filter

I. INTRODUCTION

Swarms of miniature robots (SMRs) represent a sizable group with local interactions [1] and shared objectives [2] and offer a unique solution to complex problems, inspired by natural swarms like bees, ants, termites, and fish [3]. These small and cost-effective robots collaborate using distributed control frameworks and local information sensing [4]. They overcome individual cognitive limitations, resulting in complex collective behaviors [5] and they also excel in various environments, executing tasks in parallel and showcasing cooperative capabilities [6]. Applications like fault detection, agriculture, and area inspection could greatly benefit from these swarms [7].

SMRs offer significant advantages but designing such a system poses challenges in self-organization structure, local communication, and feedback control methods [5] and conventional methods like GPS are unsuitable due to signal blockage, calibration needs, power limits, and computational limitations [6]. Communication and limited energy resources are also essential for successful operation [8].

Research on the memristor, a nano-electronic component, has shown significant potential for analog, neuromorphic, and in-memory computing applications [9], [10]. This passive device offers non-volatility, power efficiency, non-linearity, and a compact footprint with low power consumption [11]. Initially conceptualized in 1971 [12], it was first realized in 2008

This work has been partially supported by the framework of the FUN-GATERIA project, which has received funding from the European Union's HORIZON-EIC-2021-PATHFINDER CHALLENGES program under grant agreement No. 101071145 and by the project PID2022-141391OB-C22, Ministry of Science, Spain.

at HP Labs [13]. Subsequent to this, extensive research has flourished in the field, with the Conductive Bridging Random Access Memory (CBRAM) type being a strong candidate for robust, efficient, and fast fabricated devices due to its high endurance, retention, and R_{on}/R_{off} ratio. Memristors have diverse applications in oscillation-based circuits and systems, enabling investigations into brain-inspired phenomena, NP-complete problems, and bio-inspired applications [14]–[17].

This work presents a fully analog memristive circuit for collision avoidance in miniature robots, combining the oscillatory properties of RC circuits with their low-power characteristics. The design minimizes circuit area and uses a two-stage passive memristive filter, presented in Section II, for learning capabilities helping the robot become more aware of collisions in specific directions. Simulation results of Section III verify the circuit's functionality based on fabricated CBRAM devices. The paper concludes with conclusions and future work.

II. THE PROPOSED COLLISION AVOIDANCE CIRCUIT

Miniature robots require efficient operation to minimize area and power footprints, which is crucial for their overall capability and operation range with batteries. Integrating low-power memristors into a collision avoidance circuit can aid in spatial navigation, enabling self-localization in the swarm. These characteristics can be succeeded due to the sub-circuits that carry out the required signal processing derived from an ultrasonic sensor to the corresponding motor, as presented in Fig. 1(A). The main idea is to produce a pulse-width-modulated (PWM) signal with variable duty cycle. So, when the distance detected from a particular side of the robot is too small, the collision is prevented stopping the operation of the corresponding motor; a function that will be described in detail. Starting from the circuit's input from the ultrasonic sensor, it is first modulated in the Attenuation stage, in order to properly stimulate the memristive oscillator.

At the following input stages of the design, one of the most important sub-circuits of the whole design is being met; the Memristive Neuromorphic Voltage-Controlled Oscillator (MNVCO). This circuit acts as a voltage-controlled frequency modulator (VCFM), transforming the DC input acquired from the ultrasonic sensor into a spiking frequency-modulated signal with its Firing Rate (FR) representing the distance between the object and the ultrasonic sensor. This analog sub-circuit is simple enough and is based on the voltage-to-frequency conversion principle utilizing a resistor (R_{MNVCO}) in series

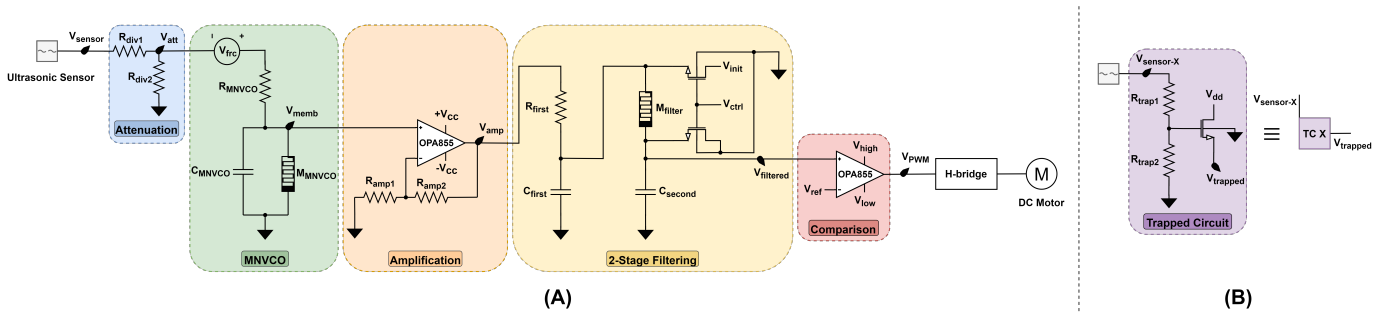


Fig. 1. (A) The proposed collision avoidance circuit with discrete processing stages. (B) A sub-circuit that produces a signal when the mini-robot is trapped.

with a parallel coupled memristor (M_{MNVCO}) and a capacitor (C_{MNVCO}) as depicted in Fig. 1(A). The utilized memristor exhibits fast unipolar switching behaviour with low voltage thresholds for low power consumption and is being described by a compact physics-based model [18], that encompasses the effects of drift, diffusion, and thermo-diffusion principles. Other than that, it has been fitted to compatible fabricated single-layer Metal-Insulator-Metal (MIM) CBRAM devices consisting of Ag ($\sim 40nm$) / SiO₂ ($\sim 20nm$) / Pt nanoparticles (NPs) ($\sim 5nm$) [19]. The MNVCO has previously been successfully fabricated with identical stoichiometry CBRAM memristors [20] and can reproduce neuron-like oscillations between the two memristor's thresholds under DC stimulation with the charging-discharging behavior of the resistor-capacitor circuit module. In this way, the instantaneous spiking frequency of the MNVCO circuit is modeled having a linear relationship with its stimulation voltage. The specifications of this sub-circuit for our test case are $R_{MNVCO} = 2.5M\Omega$ and $C_{MNVCO} = 1nF$.

Ultrasonic sensors emit pulses of ultrasonic waves and measure the time it takes for these waves to bounce off an object and return to the sensor. When the distance to the object is large, the intensity of the reflected waves decreases due to attenuation. As a result, the signal received by the sensor is weaker, leading to a lower output voltage. Typical ultrasonic sensing modules produce a maximum voltage output equal to 5V. For this reason, a voltage divider prior to the MNVCO is introduced to map the sensor's output to a proper stimulation voltage for the MNVCO sub-circuit with the resistor values equal to $R_{div1} = 100\Omega$ and $R_{div2} = 6.4\Omega$. It should be noted that these resistance values can be modified in regard to the model of the used sensor.

After the MNVCO, the signal is driven into a non-inverting operational amplifier (op-amp) in order to be amplified with the closed-loop voltage gain A_V determined by the two resistors of the feedback loop, as described by Eq. 1 below:

$$A_V = 1 + \frac{R_{amp2}}{R_{amp1}} \quad (1)$$

Given that $R_{amp2} = 9k\Omega$, and $R_{amp1} = 1k\Omega$, the gain equals $A_V = 10$. The internal op-amp parameters have been properly selected in order to model the high-speed and low-power OPA855 from Texas Instruments. The supply voltage

equals $V_{cc} = \pm 3.5V$ and its gain bandwidth product is $GBP = 8GHz$. Note that the ambient operating temperature of the circuit is considered at $T_A = 25^\circ C$. Having in mind that the next sub-circuit is a passive filter, the use of this op-amp after the MNVCO is crucial for two reasons. First and foremost, the outgoing signal from the MNVCO is quite weak and, thus, susceptible to possible noise added from the ultrasonic sensor module. Amplifying the signal before filtering can help increase the signal's amplitude relative to the noise, thereby improving the Signal-to-Noise Ratio (SNR) and the overall signal integrity. In this direction, the op-amp selected appears to have low input-referred noise that equals $e_n = 0.98nV/\sqrt{Hz}$. A higher SNR results in better filtering performance as the filter can more effectively distinguish between the wanted signal and unwanted noise. The second reason is loss compensation. Filters can introduce some signal attenuation due to their frequency response characteristics. By amplifying the signal before filtering, this loss can be compensated, ensuring that the filtered output has an adequate amplitude for being reliably processed by the next stages of the proposed circuit.

In this manner, the signal is being driven by the proposed second-order low-pass passive filter (LPF), which comprises a first conventional RC stage and a second unconventional memristive MC stage. A two-stage filter can help maintain better signal quality by allowing for a gradual and more controlled filtering process. It also helps in minimizing unwanted distortion and other side effects that might be introduced by an aggressive single-stage filter, further offering the ability to fine-tune and optimize the filtering process more precisely. It should be noted that the proposed filter has a double purpose. Its core functionality is to attenuate the high-frequency spiking signals, which directly translate to the detection of small distance values (of an object) from the sensing module. In doing so, the associated motor will halt its operation, thereby averting an impending collision. Its second task is to introduce the memory effect in a particular sensing direction so as to be more sensitive and help the respective mini-robot become increasingly aware when approaching a specific distance multiple times. This is realized by the utilization of a memristor instead of a resistor in the second stage, as its state can be slightly altered after the first stage.

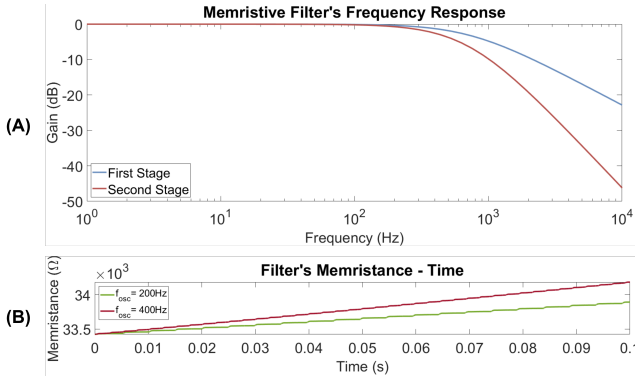


Fig. 2. (A) Frequency Response of the memristive filter after the first stage (with blue) and after the second stage (with orange) in dB. (B) The change in the filter's memristance under various oscillatory inputs.

The operation principle of this filter is now presented. At first, the memristor is SET in its low resistive state (LRS) with the help of the two NMOS FET transistors (controlled by the V_{ctrl} signal). All the transistors are simulated with a gate length of $L = 180\text{nm}$ and width $W = 9\mu\text{m}$. In the LRS the memristance of the device equals $M_{SET} = 33.4\text{k}\Omega$. The first transistor serves to provide the required voltage for the SET operation to the top electrode of the device, while the second transistor ensures that during this procedure the bottom electrode of the device will be grounded. After that, and with the arriving oscillations from the previous sub-circuit, a negative voltage difference is applied to the memristor, gradually forcing it to RESET its state and proportionally increasing its memristance as seen in Fig. 2(B). As an example, a slew rate of $4.76\Omega/\text{ms}$ is observed in response to a spiking input with a frequency of 200Hz , and a corresponding rise with $7.57\Omega/\text{ms}$ for an input with a frequency of 400Hz . This memristance increment results in lowering the cut-off frequency of the filter, resulting in a more aggressive filtering behavior, thus preventing the collision in the corresponding direction. The cut-off frequency f_c of the filter is given by the following Eq. 4:

$$f_c = \frac{1}{2\pi\sqrt{R_{first}M_{filter}C_{first}C_{second}}} \quad (2)$$

and its design parameters are equal to $R_{first} = 1\text{k}\Omega$, $M_{filter} = M_{SET} = 33.4\text{k}\Omega$, $C_{first} = 220\text{nF}$, and $C_{second} = 7\text{nF}$, offering a cut-off frequency that equals $f_c = 701.7\text{Hz}$, as Fig. 2(A) showcases. Note that the filter's slope after the cut-off frequency is -20dB/Decade for the first stage and -40dB/Decade for the second stage.

The final stage of the proposed design is tasked with amplifying the signal to facilitate motor actuation. This stage incorporates an op-amp (with identical internal design parameters as employed in the Amplification stage), serving as a comparator; the filtered signal is compared to a DC reference voltage, denoted as V_{ref} . When the input signal amplitude exceeds this reference voltage, the output maintains a constant amplitude V_{high} . Conversely, when the input signal falls below

this threshold, the output provides the value V_{low} , thereby generating a PWM control signal as the following Eq. 3 describes:

$$V_{PWM} = \begin{cases} V_{high}, & V_{filtered} \geq V_{ref} \\ V_{low}, & V_{filtered} < V_{ref} \end{cases} \quad (3)$$

In such applications, DC motors are preferred due to their small dimensions, weight, ease of control, and reliability. For our test case, we assume that our circuit will drive the Faulhaber's 2224U006SR motor with a nominal voltage of 6V , as it has been utilized in this kind of applications [21], [22]. In order to achieve steady-speed operation of such a DC motor without fluctuations driven by a PWM signal (commonly known as *PWM whine* phenomenon), its minimum control frequency is given by the Eq. 4:

$$f_{min} \geq \frac{5}{2\pi\tau} \quad (4)$$

where τ is the time constant of the motor. In our case, this is $\tau = 11\text{ms}$, so the minimum control frequency of the PWM signal occurs to be $f_{min} \geq 72.34\text{Hz}$, also justifying the circuit parameters selected. In any other case where another motor model is utilized, the design parameters of the circuit may change. The designated voltage values have been chosen as follows: $V_{ref} = 1.86\text{V}$, $V_{high} = 4\text{V}$, and $V_{low} = 0\text{V}$. Consequently, the generated signal consists of a PWM signal between 0V and 3.5V . Its duty cycle is higher at low spiking frequencies, as seen in Fig. 3(E), forcing the motor to run at a higher speed. $V_{frc} = 220\text{mV}$ forces the MNVCO to generate oscillations even though the output from the ultrasonic sensor is 0V . In this way, the operation of the motor is ensured even when no object is near and the mini-robot can move without interrupting its trajectory.

Besides the previously presented circuit, another one has been developed to address these situations in which the robot becomes trapped, depicted in Fig. 1(B). Within this sub-circuit, the input signal V_{sensor} is subjected to appropriate attenuation using a voltage divider with defined parameters: $R_{trap1} = 100\Omega$ and $R_{trap2} = 25\Omega$. This attenuated signal is then employed to modulate the gate of a NMOS transistor, inducing its activation when the signal exceeds its threshold. Consequently, a voltage $V_{trapped}$ is seen at the transistor's source terminal, serving as an indicator that the proximity between the object and the sensing module has reached a critical level. The voltage supplying this transistor is $V_{dd} = 1.5\text{V}$.

III. SIMULATION RESULTS

The designed circuit has been rigorously validated through simulations conducted with the Cadence Virtuoso Design Suite. All pivotal signal processing stages are illustrated in Fig. 3, tracing the transformation of the input signal from the ultrasonic sensor to the resultant PWM control signal.

In Fig. 3(A), it becomes evident that the output from the ultrasonic sensor experiences attenuation (producing the V_{att} voltage) due to the voltage divider implemented in the

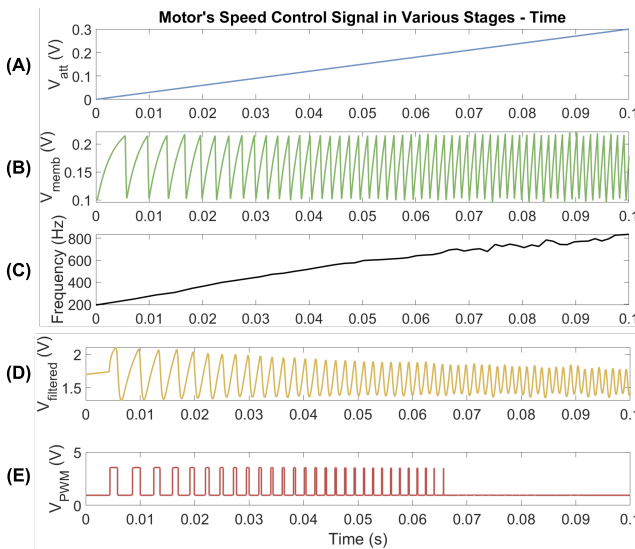


Fig. 3. Processed sensor's signal after (A) Attenuation, (B) MNVCO, (D) 2-Stage Filtering, and (E) Comparison Stage. (C) Frequency output after MNVCO stage.

initial stage, as shown in Fig. 1(A), in order to properly define the oscillation frequency range of the MNVCO. Subsequently, the oscillator generates a spiking signal V_{memb} (name taken from the bio-inspired membrane potential of a neural cell), with a frequency response directly proportional to its stimulation voltage (being the summation of the V_{att} and V_{frc}), as corroborated by Figs. 3(B) and (C). Following amplification, the signal undergoes filtration by the two-stage passive memristive filter described in Section II, with its output depicted in Fig. 3(D). This filter diminishes signal amplitude at higher frequencies, thus preventing motor operation in situations of close object proximity. After that, the signal is fed into a comparator, producing the desired PWM control signal represented in Fig. 3(E). Finally, this is the input of an H-bridge (typically the well-known L298N driver module) in order to drive the motor with the required power, as these driving modules can offer high output currents and protection features at the same time to ensure the safe operation of the motor. The proposed circuit's mean power consumption is 117.73mW, and its compactness can save space and weight compared to using a power-consuming micro-controller like Arduino for the generation of the PWM control signal.

In addition to the aforementioned signal processing, it is imperative to elucidate the mechanism behind the generation of the alert signal, employing multiple ultrasonic sensors. As depicted in Fig. 4(A), a top view of a mini-robot is provided, equipped with four ultrasonic sensors for each cardinal direction. Each module is linked to its respective motor, governing the robot's movement in the corresponding direction due to each PWM's duty cycle and integrating the circuit delineated in Fig. 1(A). To elaborate, the outputs from these ultrasonic sensors are individually directed to four discrete sub-circuits within Fig. 1(A), further leading to the speed control of the corresponding motors. In parallel, they also serve as inputs to

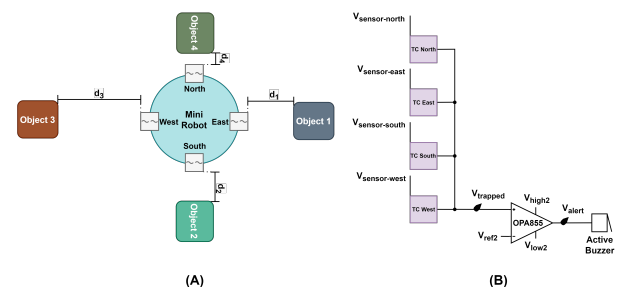


Fig. 4. (A) Topology of four ultrasonic sensors in a mini-robot. (B) The connectivity required for the sub-circuit of Fig. 1(B) for the generation of an alert signal in case that the mini-robot is being trapped.

four distinct sub-circuits presented in Fig. 1(B) to facilitate the generation of the alert signal, as exemplified in Fig. 4(B).

In situations where the trapped signal's amplitude exceeds $V_{ref2} = 1V$, it signifies that the mini-robot is entrapped by its neighbors, indicative of the close proximity and minimal distances d_1 through d_4 . The voltage supply values for the utilized op-amp in Fig. 4(B) are $V_{high2} = 5.5V$ and $V_{low2} = 0V$. In Fig. 5, a test case of this is plotted for continuously decreasing distances (thus increasing sensors' voltages) around the mini-robot. The generated V_{alert} signal can be further utilized in order to activate an active buzzer informing about the trapped situation of the mini-robot.

IV. CONCLUSIONS AND FUTURE WORK

In summary, this work introduces a novel memristive circuit for collision avoidance to efficiently process ultrasonic sensor signals, preventing collisions and enhancing mini-robots' capabilities. The circuit's memory capabilities improve mini-robots' awareness, and simulation results validate its functionality for real-world applications.

In future work, the proposed circuit can be improved with in-hardware machine learning characteristics, enhancing mini-robot's movement efficiency. This can be achieved through microphones receiving alert signals from trapped robots, and using sound-localization techniques the mini-robots can modify their trajectory.

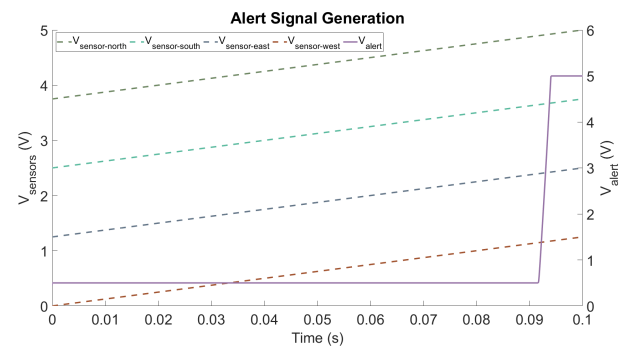


Fig. 5. Output voltages of the four sensors related with the distances d_1 to d_4 of the Fig. 4(A) (left y axis). The produced alert signal generated from the circuit depicted in Fig. 4(B) (right y axis).

REFERENCES

- [1] J. Yang and Y. Shi, "Adaptive Coordinated Motion Control for Swarm Robotics Based on Brain Storm Optimization," in *2021 11th International Conference on Information Science and Technology (ICIST)*, 2021, pp. 444–451.
- [2] A. R. Cheraghi, S. Shahzad, and K. Graffi, "Past, Present, and Future of Swarm Robotics," in *Intelligent Systems and Applications*, K. Arai, Ed. Springer International Publishing, 2022, pp. 190–233.
- [3] M. Patil, T. Abukhalil, S. Patel, and T. Sobh, "Hardware Architecture Review of Swarm Robotics System: Self Reconfigurability, Self Reassembly and Self Replication," in *Innovations and Advances in Computing, Informatics, Systems Sciences, Networking and Engineering*, T. Sobh and K. Elleithy, Eds. Springer International Publishing, 2015, pp. 433–444.
- [4] M. Dorigo, G. Theraulaz, and V. Trianni, "Swarm Robotics: Past, Present, and Future [Point of View]," *Proceedings of the IEEE*, vol. 109, no. 7, pp. 1152–1165, 2021.
- [5] H. Duan, M. Huo, and Y. Fan, "From animal collective behaviors to swarm robotic cooperation," *National Science Review*, vol. 10, no. 5, p. nwad040, 02 2023.
- [6] M. Duan, X. Lei, Z. Duan, and Z. Zheng, "A Minimalist Self-Localization Approach for Swarm Robots Based on Active Beacon in Indoor Environments," *Sensors*, vol. 23, no. 10, 2023.
- [7] M. Schranz, M. Umlauft, M. Sende, and W. Elmenreich, "Swarm robotic behaviors and current applications," *Frontiers in Robotics and AI*, p. 36, 2020.
- [8] Z. Hao, S. Mayya, G. Notomista, S. Hutchinson, M. Egerstedt, and A. Ansari, "Controlling Collision-Induced Aggregations in a Swarm of Micro Bristle Robots," *IEEE Transactions on Robotics*, vol. 39, no. 1, pp. 590–604, 2023.
- [9] E. Tsipas, T. P. Chatzinikolaou, K.-A. Tsakalos, K. Rallis, R.-E. Karanmani, I.-A. Fyrigos, S. Kitsios, P. Bousoulas, D. Tsoukalas, and G. C. Sirakoulis, "Unconventional computing with memristive nanocircuits," *IEEE Nanotechnology Magazine*, vol. 16, no. 6, pp. 22–33, 2022.
- [10] T. P. Chatzinikolaou, I.-A. Fyrigos, V. Ntinias, S. Kitsios, P. Bousoulas, M.-A. Tsompanas, D. Tsoukalas, A. Adamatzky, and G. C. Sirakoulis, "Wave Cellular Automata for Computing Applications," in *2022 IEEE International Symposium on Circuits and Systems (ISCAS)*, 2022, pp. 3463–3467.
- [11] H. Duan, S. Cheng, L. Qin, X. Zhang, B. Xie, Y. Zhang, and W. Jie, "Low-Power Memristor Based on Two-Dimensional Materials," *The Journal of Physical Chemistry Letters*, vol. 13, no. 31, pp. 7130–7138, 2022.
- [12] L. Chua, "Memristor-the missing circuit element," *IEEE Transactions on Circuit Theory*, vol. 18, no. 5, pp. 507–519, 1971.
- [13] D. B. Strukov, G. S. Snider, D. R. Stewart, and R. S. Williams, "The missing memristor found," *nature*, vol. 453, no. 7191, pp. 80–83, 2008.
- [14] I. K. Chatzipaschalidis, E. Tsipas, I.-A. Fyrigos, A. Rubio, and G. C. Sirakoulis, "Cbram-based bio-inspired circuit for the emulation and treatment of the parkinson's disease," *IEEE Transactions on Circuits and Systems II: Express Briefs*, 2023.
- [15] T. P. Chatzinikolaou, I.-A. Fyrigos, V. Ntinias, S. Kitsios, P. Bousoulas, M.-A. Tsompanas, D. Tsoukalas, A. Adamatzky, and G. C. Sirakoulis, "Wave Cellular Automata for Computing Applications," in *2022 IEEE International Symposium on Circuits and Systems (ISCAS)*, 2022, pp. 3463–3467.
- [16] V. Ntinias, I. Vourkas, G. C. Sirakoulis, and A. Adamatzky, "Mimicking Physarum Space Exploration with Networks of Memristive Oscillators," in *Handbook of Memristor Networks*. Springer, 2019, pp. 1241–1274.
- [17] T. P. Chatzinikolaou, I.-A. Fyrigos, R.-E. Karanmani, V. Ntinias, G. Dimitrakopoulos, S. Cotofana, and G. C. Sirakoulis, "Memristive oscillatory circuits for resolution of np-complete logic puzzles: Sudoku case," in *2020 IEEE International Symposium on Circuits and Systems (ISCAS)*. IEEE, 2020, pp. 1–5.
- [18] I.-A. Fyrigos, T. P. Chatzinikolaou, V. Ntinias, S. Kitsios, P. Bousoulas, M.-A. Tsompanas, D. Tsoukalas, A. Adamatzky, A. Rubio, and G. C. Sirakoulis, "Compact thermo-diffusion based physical memristor model," in *2022 IEEE International Symposium on Circuits and Systems (ISCAS)*. IEEE, 2022, pp. 2237–2241.
- [19] P. Bousoulas, D. Sakellaropoulos, C. Papakonstantinopoulos, S. Kitsios, C. Arvanitis, E. Bagakis, and D. Tsoukalas, "Investigating the origins of ultra-short relaxation times of silver filaments in forming-free SiO_2 -based conductive bridge memristors," *Nanotechnology*, vol. 31, no. 45, p. 454002, 2020.
- [20] P. Bousoulas, C. Tsouatas, J. Hadfield, V. Aslanidis, S. Limberopoulos, and D. Tsoukalas, "Low power stochastic neurons from sio 2-based bilayer conductive bridge memristors for probabilistic spiking neural network applications—part i: Experimental characterization," *IEEE Transactions on Electron Devices*, vol. 69, no. 5, pp. 2360–2367, 2022.
- [21] J. Wu, J. Cai, L. Fan, M. Huo, and Z. Zheng, "Design and algorithm research of high speed two-wheeled mini robots," *Sensors & Transducers*, vol. 25, p. 189, 2013.
- [22] M. A. Armada, P. de González Santos, M. Han, P. Kopacek, B. Putz, E. Sshierer, and M. Würzl, "Mobile mini robots for mas," in *Climbing and Walking Robots: Proceedings of the 7th International Conference CLAWAR 2004*. Springer, 2005, pp. 201–209.